

- ⁷G. Ziebarth, *Z. Phys.* **212**, 330 (1968).
⁸D. A. Shirley, in *Hyperfine Structure and Nuclear Radiations*, edited by E. Matthias and D. A. Shirley (North-Holland, Amsterdam, 1968), p. 979.
⁹V. Jaccarino, in *Magnetism*, edited by G. T. Rado and H. Suhl (Academic, New York, 1965), Vol. II a, p. 307.
¹⁰M. E. Lines and E. D. Jones, *Phys. Rev. A* **130**, 1313 (1965).
¹¹M. E. Lines and E. D. Jones, *Phys. Rev.* **141**, 525 (1966).
¹²J. C. Love, F. E. Obenshain, and G. Czjzek, *Phys. Rev. B* **3**, 2827 (1971).
¹³R. L. Cohen, G. K. Wertheim, A. Rosencwaig, and H. J. Guggenheim, *Phys. Rev. B* **5**, 1037 (1972).
¹⁴J. F. Herbst, D. N. Lowy, and R. E. Watson *Phys. Rev. B* **6**, 1913 (1972).
¹⁵J. S. Van Wieringen, *Discuss. Faraday Soc.* **113**, 118 (1955).

PHYSICAL REVIEW B

VOLUME 7, NUMBER 6

15 MARCH 1973

Inelastic-Electron-Tunneling Spectroscopy of Metal-Insulator-Metal Junctions*

J. Klein, A. Léger, M. Belin, and D. Défourneau
*Groupe de Physique des Solides de l'Ecole Normale Supérieure,
 Laboratoire associé au Centre National de la Recherche Scientifique,
 Tour 23, Université de Paris VII, Paris 5e, France*

M. J. L. Sangster

J. J. Thomson Physical Laboratory, University of Reading, Reading, United Kingdom
 (Received 28 June 1972)

The inelastic tunneling of electrons in a metal-insulator-metal junction has been shown to be a spectroscopic method for studying the vibrational modes of the whole system. In the present paper we consider the possibility of deducing precise information from this spectroscopy. The low-voltage part of the spectrum (i. e., the d^2I/dV^2 -vs- V characteristic) gives information about the phonons of the electrodes. The phonon density, which is deduced for a Mg electrode, is critically compared with the density deduced from neutron scattering. The range of this phonon probe is then studied by tunneling into multilayer electrodes. The 40–90-meV range of the characteristic of a Mg-Pb junction exhibits a specific structure due to the lattice vibrations of the insulator. This structure is compared with the infrared spectrum and the phonon density of states of MgO, as well as with a theoretical calculation of the tunneling current in the transfer-Hamiltonian formalism. From the fit obtained, it is deduced that the 30-Å-thick insulator, grown on Mg, is an oxide, in contrast with the insulator grown on Al, which was previously deduced to be a hydroxide. At higher energies (100–500 meV), the vibrational spectrum of molecules contained in the insulator region is observed. The identification of the lines is shown to be accurate and it gives precise information on these molecules, especially about their chemical binding with the insulator. This last point could be important in the future for studying the problem of adsorption on solid surfaces.

I. INTRODUCTION

A new field in the study of tunneling in metal-insulator-metal (MIM) junctions was devised in 1966 by Jaklevic and Lambe.^{1,2} They observed structures in the d^2I/dV^2 characteristics which were related to vibrational excitations of molecular impurities contained in the insulator. Since that date a considerable amount of work has been devoted to the subject. It has been found that the phenomenon is more general than was at first thought, because vibrational modes of the metallic electrodes^{3,4} and of the insulating barrier itself^{5–7} have also been observed.

The physical origin of these structures is mainly due to the inelastic tunneling of electrons.⁸ An electron can cross the potential barrier of the insulator by (elastic) tunneling with conservation of its energy. But this barrier potential may contain dynamic terms, such as those due to the vi-

brational modes of the insulator. Then an electron also has the possibility of going from one electrode to the other, exciting one mode of vibration, and losing the corresponding energy $\hbar\omega_0$. Clearly, this can happen only when the applied voltage is greater than $V_0 = \hbar\omega_0/e$. This gives the threshold for the new process to occur. Above this applied voltage the total probability of crossing the barrier, for an electron at the Fermi level, is the sum of the elastic and inelastic probabilities, and the conductance is increased (see Fig. 1).

Actually, the inelastic tunneling of electrons involves the vibrational spectroscopy of the whole MIM system. In the present paper we report new results on the topic, mainly on structures in which the identification can be carried out with more precision. We also try to give answers to various questions which have been raised on the subject.

We have studied particularly Mg-MgO-Pb junctions because, in that structure, the completeness

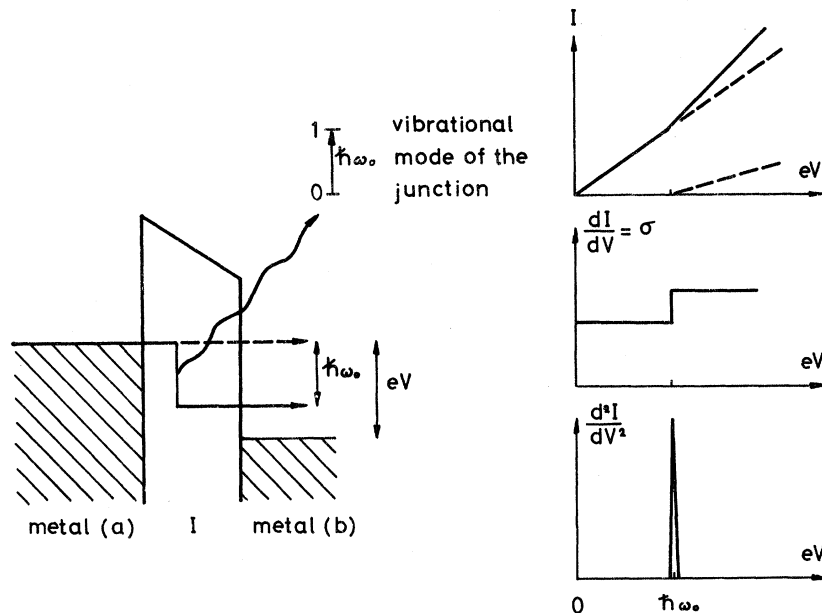


FIG. 1. Inelastic electron tunneling: energy diagram for a process during which a vibrational mode of energy $\hbar\omega_0$ is excited. Corresponding current characteristics.

of the spectroscopy is well demonstrated: The different vibrational modes of the component parts of the whole system are observed. Moreover, those different modes are conveniently separated in energy. In fact, this separation is observed in most MIM systems, for more general reasons. The phonons of the metals lie at low energy (0–40 meV in this system), as the atomic masses are generally fairly heavy and the metallic bond is rather weak. The vibrations of the insulators are at higher energies (0–90 meV in MgO), as the bonds between atoms are strong in those ionic or covalent solids. The molecular impurities of the insulator generally include hydrogen, and the corresponding vibrations are at still higher energies (up to 450 meV) because the bond is strong and the hydrogen mass is very light. This leads to an easy separation of the observed spectra.

In Sec. II we discuss the experimental limitations of resolution in the spectroscopy, arising from the thermal broadening and the second-derivative technique. This last discussion is valid for any dynamic method which uses a finite modulation to get the derivative of a characteristic. Since, as we have seen, the modes of the different parts of the MIM junction have distinct energies, we then examine the tunnel characteristics at increasing energies. In Sec. III the electrode phonon structure is described, with emphasis on the depth in the metal which is probed by the tunneling current. The observation of the phonons of the insulator is reported in Sec. IV. A comparison between the observed spectrum and an explicit calculation of the inelastic current is attempted using phonon data obtained from neutron scattering.

We support the spectrum identification of the oxide with an $O^{16} - O^{18}$ isotopic effect. Section V is devoted to the spectroscopy of the molecular impurities in the barrier. We first present a detailed study of the spectrum obtained with formic acid which gives us precise information about the bounding of these molecules with the matrix. An accurate measurement of the $H^1 - H^2$ isotopic effect on the OH stretching mode in Mg-Pb junction is then made, throwing light on the precision that can be reached in this spectroscopy. Ultimately we study the effect of superconducting electrodes on the line shape of a well-defined inelastic-tunneling peak.

II. RESOLUTION IN TUNNELING SPECTROSCOPY

The second derivative d^2I/dV^2 vs V is generally measured, as it is the most interesting characteristic (see Fig. 1). First, it strongly reduces the effect of elastic processes as they give a current which is roughly linear with applied voltage, and second, at least in some cases,⁸ it gives directly the spectral weight function $D(E)$ of the modes. Let us consider the experimental resolution that we can expect on that characteristic, as this determines the performance of this kind of spectroscopy. Besides the intrinsic linewidth of the peaks, some broadening may appear for several reasons, which we shall now discuss.

A. Thermal Broadening

This effect has been studied in detail by Lambe and Jaklevic.² At finite temperature, and for electrodes in the normal state, the inelastic current is given by

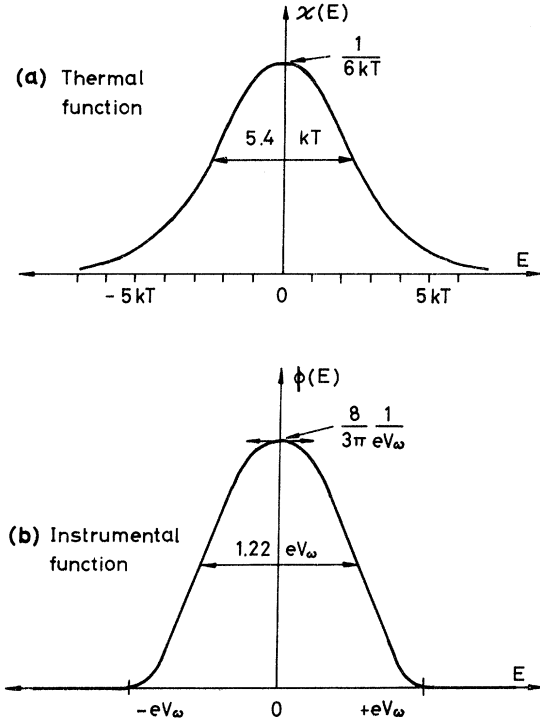


FIG. 2. Experimental broadening of the lines. (a) Finite temperature effect: For normal electrodes, the second derivative of the tunneling current is the convolution product of the spectral weight function of the vibrator by the function $\chi(E)$. (b) Finite voltage modulation effect: The experimental plot of the second harmonic of the current is the convolution product of the second derivative of the current function by the function $\phi(E)$. As expected, $\phi(E)$ is zero outside of the interval $-eV_\omega$, eV_ω , which corresponds to the voltage modulation.

$I_{1\text{ne1}} = C \iint f(E)[1 - f(eV - \hbar\omega_0 + E)]D(\hbar\omega_0)dEd(\hbar\omega_0)$, where C is a constant depending upon the junction, $f(E)$ is the Fermi-Dirac function, and $D(\hbar\omega_0)$ is the spectral weight function. They have shown that $d^2I/d(eV)^2$ is a convolution product of the spectral weight function $D(\hbar\omega_0)$ with the thermal function $\chi(E)$ represented in Fig. 2(a):

$$\frac{d^2I}{d(eV)^2} = D * \chi, \quad (1)$$

where

$$\chi(E) = \frac{1}{kT} e^x \frac{(x-2)e^x + x + 2}{(e^x - 1)^3} \quad [\text{with } x = (E/kT)].$$

The half-width of the thermal function is $5.4kT$. Hence, if a given resolution is desired, there is an upper limit to the temperature at which the experiment can be performed.

When one uses superconducting electrodes, the result cannot be expressed as a convolution. But there is a gap Δ in the density of states of the

superconductor, and, as the ratio Δ/kT increases, the thermal effects are very rapidly eliminated because the tail of the Fermi-Dirac function is now cut off for energies smaller than Δ . However, in this case, even in the low-temperature limit, d^2I/dV^2 does not give $D(E)$ directly, as we shall see later on.

B. Broadening because of Finite-Modulation Technique

To get the second derivative, $d^2I/d(eV)^2$, a dynamical technique is used. A finite modulation of the voltage is applied, and the second harmonic of the current is detected. Let us consider the broadening introduced in such a procedure.

We call $f''(eV)$ the exact second derivative and $F''(eV)$ the function obtained experimentally. The resulting current is a function of time:

$$I = f(eV_0 + eV_\omega \cos \omega t),$$

where $I = f(eV)$ is the junction characteristic and eV_ω the modulation amplitude at frequency ω . The second harmonic is detected:

$$I_{2\omega} = \frac{2}{\tau} \int_{-\tau}^{\tau} f(eV_0 + eV_\omega \cos \omega t) \cos 2\omega t dt.$$

Substituting the new variable $E = eV_\omega \cos \omega t$, two partial integrations give

$$\frac{\pi}{2} V_\omega^2 I_{2\omega} = \int_{-eV_\omega}^{eV_\omega} f''(eV_0 + E) \frac{(e^2 V_\omega^2 - E^2)^{3/2}}{3} dE.$$

It then appears that the experimental quantity, $F'' = (4/V_\omega^2)I_{2\omega}$, is a convolution product of the exact second derivative, $f'' = d^2I/d(eV)^2$, with an instrumental function ϕ which is represented in Fig. 2(b):

$$F'' = f'' * \phi, \quad (2)$$

where

$$\phi(E) = \frac{8}{3\pi} \frac{1}{(eV_\omega)^4} (e^2 V_\omega^2 - E^2)^{3/2} \quad \text{for } |E| < eV_\omega$$

$$= 0 \quad \text{for } |E| > eV_\omega.$$

The half-width of the instrumental function is $1.22V_\omega$, and, as expected, it is zero out of the interval $-eV_\omega$, eV_ω .

Then, the modulation amplitude must be adjusted to give the resolution which is required, and a delicate compromise must be found, as the signal-to-noise ratio decreases as V_ω^2 . One might think of inverting Eq. (2) to get the exact characteristic f'' , but this would need perfect knowledge of the function F'' , which is impossible because of the experimental noise.

III. PHONONS OF ELECTRODES LATTICE (0-40 meV)

The observation of structure on d^2I/dV^2 related to the phonon spectrum of the electrode has been

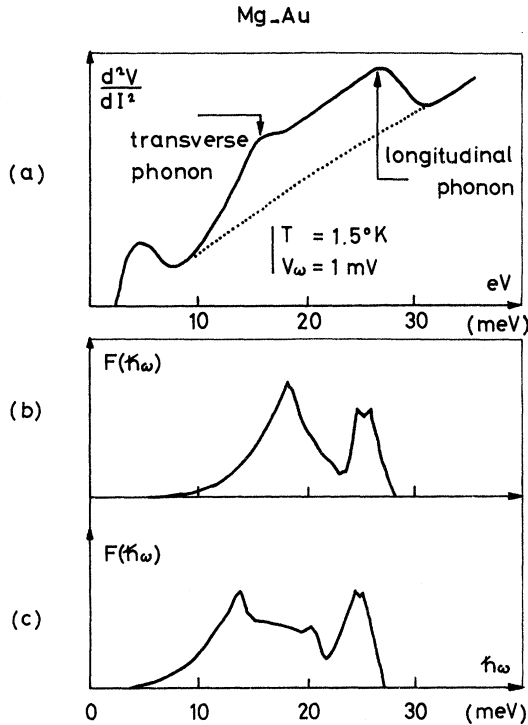


FIG. 3. (a) d^2V/dI^2 characteristic of a Mg-Au junction showing the phonon structure of the (normal-metal) Mg electrode. Phonon density of states, deduced from a central-force model (b) and a tensor-force model (c), fitted to neutron-scattering data. As is outlined in the text, the phonon density of states deduced from neutron experiments is rather model dependent.

done earlier for different metals³: Al, Pb, Sn, In, etc. In the present paper, we have specially studied the case of Mg-*X* junction, as it is instructive.

A. Phonon of Magnesium

The first experiment on Mg electrodes is due to Adler⁴ on Mg-MgO-Mg (or Al) junctions. In his experiment, only the longitudinal peak was resolved. This observation seemed to suggest that the electron coupling to the transverse-phonon modes was much weaker than that to the longitudinal ones. However, the experimental resolution for a given structure depends strongly on the background. In our experiment we have carried out measurements on clean Mg-MgO-Au junctions. The results are shown in Fig. 3(a). In this kind of junction, the background is specially smooth and thus the transverse- and longitudinal-phonon peaks of Mg (16 and 27 meV) can both be easily identified.⁹ This indicates an analogous coupling strength to the two modes. The phonons of Au give a weaker structure which is not seen here.

Actually, it seems hazardous to speculate on

what quantity one measures exactly since the theoretical calculations¹⁰ are not yet explicit. Nevertheless, the main part of the structure is symmetrical and probably has its origin in an inelastic process.¹⁰ Moreover, it seems to be closely related to the phonon density of states $F(\omega)$ of the metal, and so we assumed that the second derivative of the tunnel current is proportional to that function $F(\omega)$. We can then compare our results to the Mg phonon density of states deduced from neutron-scattering data.¹¹ This is done in Fig. 3. Clearly, the spectrum obtained from the neutron experiment is quite model dependent: Whether a central-force or a tensor-force model is used to interpolate the dispersion relations $\omega(\vec{k})$ obtained for high-symmetry directions, Young and Koppel¹¹ found, respectively, 18 and 14.5 meV for the transverse-phonon peak. Our experimental value is 16 meV. For the longitudinal phonon, both models give 27 meV and our data agree well with this value.

Therefore, tunneling in normal metals appears to be a competitive method to get the phonon density of states, at least in the case of magnesium. In fact, such an assumption was made previously in an experiment on granular aluminium¹² and was fruitful in explaining the T_c enhancement mechanism in that material.

B. Range of Inelastic-Tunneling Probe in Electrodes

It is interesting to know the depth to which the phonons of the electrodes are detected in a tunneling experiment. In order to give an answer to this question, we have made junctions M-I-M₁-M₂ and tried to observe the phonons of M₂ for different thicknesses of M₁. Nonmiscible metals {1} and {2} must be used to have a well-defined interface. We find that the results depend completely upon the relative values of the two Debye temperatures Θ_1 and Θ_2 .

Figure 4 gives the result for a hard metal backed by a soft one: Ag-Pb ($\Theta_1 \sim 215$ °K, $\Theta_2 \sim 90$ °K). We have plotted the tunneling characteristic for different thicknesses (d) of the silver film (50–300 Å). These films are deposited at 77 °K to ensure continuity, but, in fact, the results are meaningful only for d greater than 100 Å, as it is only in those cases that electron microscopy indicates an optical continuity of the film. As it can be seen in curve (b), the phonons of Pb (in the normal state) are clearly observed through the Ag. Moreover, the strength of this structure, $\delta\sigma/\sigma$, does not decay significantly as d increases in this range of thickness [curve (a)]. {This independence with d is in contrast with the dependence on d of the strong-coupling structure when Pb is superconducting [curves (a) and (c)]—this last point being a check that the current is not just

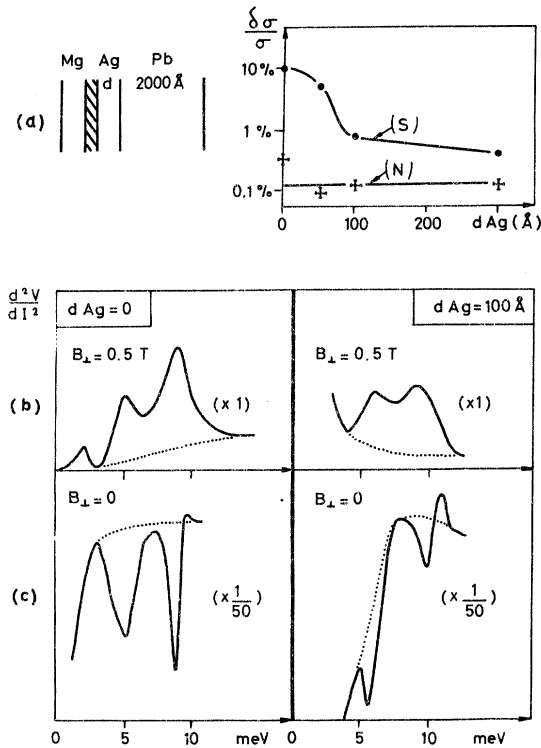


FIG. 4. Tunneling observation of the phonons of a Pb film, through an Ag film. Curves (a) represent the strength of the Pb phonon structure vs the thickness of the Ag film—when Pb is in the normal state (N) and when it is in the superconducting state (S). The experimental plots of the d^2V/dI^2 characteristics are reported, for two thicknesses of the Ag film, for normal Pb [curves (b)] and superconducting Pb [curves (c)] (the experimental temperature is 1.5°K, the modulation 1 mV). Clearly, the observation of the phonon structure of Pb in the normal state is not much affected by the presence of an Ag film (at least for Ag thickness up to 300 Å). Although it has quite a different origin, the phonon structure due to the superconducting state is shown for purposes of comparison—it decreases very rapidly as the Ag film thickness increases.

flowing through holes in the Ag film.}

Figure 5 shows results for a M-I-Pb-Al junction with a 300-Å-thick Pb film. Here the situation, as regards the Debye temperatures, is reversed ($\Theta_1 \sim 90^\circ\text{K}$, $\Theta_2 \sim 400^\circ\text{K}$), and the experimental results are quite different. The phonon structure due to Al is *not* observable through Pb. Quantitatively, its strength has been reduced by a factor of at least 10 from the situation without Pb.

These two experiments indicate that the phonons of metal (2) can be observed through metal {1} only if the phonon of {2} can propagate in {1}. This is the case when the high-frequency cutoff of vibrations in M_1 ($k\Theta_1/\hbar$) has a higher values than in M_2 ($k\Theta_2/\hbar$).¹³ In conclusion, *the inelastic tunneling appears to be a short-range probe* of the phonons

of the electrodes (300 Å or less). To be detected, a vibrational mode must give a finite amplitude on the first atomic layers of the electrode. This experimental conclusion is in agreement with the theoretical work of Ref. 9.

IV. PHONON SPECTRUM OF BARRIER LATTICE (0–90 meV)

A. Experimental Results

We have studied the characteristics of a Mg-MgO-Pb junction in the 30–100-meV range. The samples were made by evaporation of Mg at 10^{-7} Torr in a bell jar which was initially cleaned by ionic bombardment. The oxidation of Mg is carried out in a glow discharge established in a stream of pure oxygen, and the Pb counter electrode is evaporated.

The experimental plot is shown in Fig. 6(a). It shows structure with four well-defined peaks at 38, 54, 66, and 82 meV. The maxima at 38 and 66 meV are not very strong, and on some samples they are not observed as peaks but rather as shoulders on the experimental curve. However the main peaks at 54 and 82 meV are always strong. The total structure corresponds to a conductivity increase $\delta\sigma/\sigma$ of about 0.3%. In previous experiments^{5,6} performed on Mg, no clear structure due to MgO was observed but only a peak at about 85 meV.⁶ A possible explanation for the results of Ref. 5 is that the barrier was partly made with hydroxide and carbonate because of the room-air oxidation of Mg. In Ref. 6 the oxide was prepared in a glow discharge, but the junction

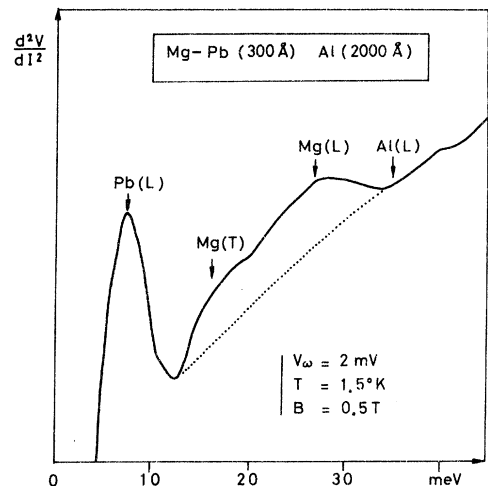


FIG. 5. Attempt to observe the phonons of an Al film through a 300-Å-thick Pb film. The d^2V/dI^2 characteristic shows the phonon structure of the injecting electrode (Mg) and of the thin Pb film, but nothing is observed at the energy of the Al phonons. This situation is in contrast with the situation reported in Fig. 4, as pointed out in the text.

considered was Mg-MgO-Mg and the rapid variation of the conductance background may have obscured the structure.

Recently Jaklevic and Lambe⁷ have looked for the barrier-lattice modes in junctions with yttrium and chromium oxides. They have compared the spectra obtained with optical absorption measured

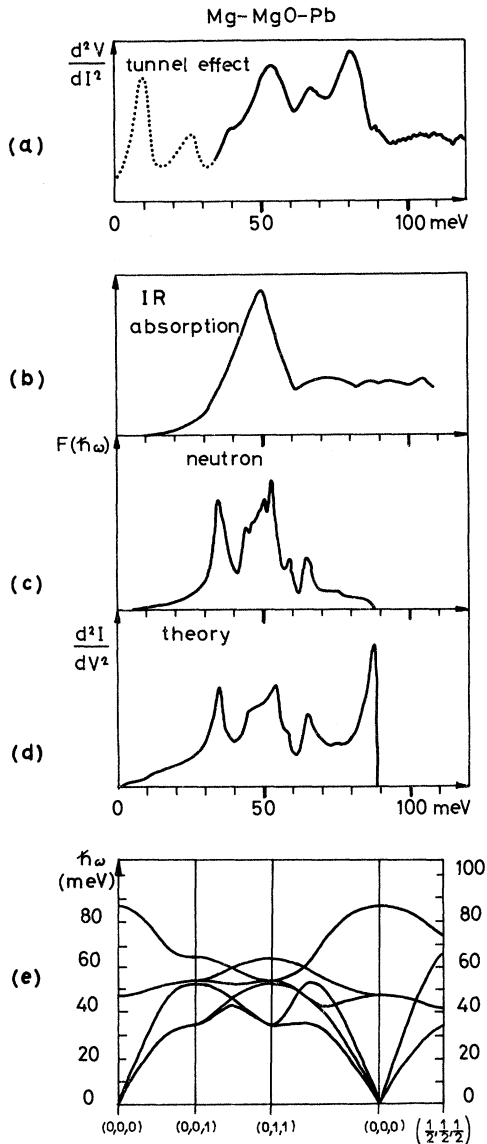


FIG. 6. Phonon structure of a MgO barrier lattice. (a) Experimental d^2V/dI^2 characteristic for a Mg-MgO-Pb junction. The beginning of the curve is dotted because it corresponds to the phonon structure of the electrodes. The full line is specific of MgO. This tunneling spectrum is compared to other types of spectrum on MgO: (b) Infrared absorption of MgO; (c) Phonon density of states as deduced from neutron-scattering experiment; (d) Theoretical spectrum calculated in the present paper; (e) Dispersion relations of phonons in MgO from neutron-scattering experiments.

directly on their oxide film. This was necessary because, in the literature, data are given for the crystalline oxide and not for the amorphous oxide which probably grows at the metal surface. In these conditions, their comparison exhibits clear correlations between the two spectra. The case of MgO is somewhat different because this oxide is crystalline, as it is an ionic material. Then the results can be easily compared with the data of the literature. Moreover, these data are available from different types of experiments; infrared absorption and neutron scattering. So a more detailed analysis of the tunneling curves can be attempted.

A direct comparison between the tunneling spectrum [Fig. 6(a)] and the infrared (IR) absorption curve [Fig. 6(b)] can be made. The IR absorption spectrum exhibits a single peak at 50 meV. The selection rules in optics allow the excitation only for phonons which are optical and transverse, with zero wave vector. That this is the case in MgO can be checked from the dispersion curves [Fig. 6(e)]. But clearly, in inelastic tunneling the selection rules must be different as the fit between the two spectra is poor.

Another possibility is to make a comparison of the tunneling curve with the total phonon density of states, as deduced from the neutron studies performed on MgO by one of the authors and co-workers.¹⁴ By neutron scattering, dispersion curves $\hbar\omega(\vec{k})$ are obtained for high-symmetry directions; then, thanks to a breathing-shell model fitting those energies, the energies and the eigenvectors are calculated for any wave vector \vec{k} , and the density of states is deduced. The corresponding curve is shown in Fig. 6(c). Again, the fit is rather poor: in the high-energy part of spectrum, the density of states is low, but we observe a strong peak in the tunneling curve. In fact, this is not very surprising as it corresponds to LO modes which are expected, in an ionic material, to be strongly coupled to electrons.

Then we can try to make an explicit calculation of the inelastic-tunneling current and see if the fit between such a calculated spectrum and the experimental one is better than the previous ones.

B. Calculation of Barrier-Phonon Effect

We shall use the transfer-Hamiltonian¹⁵ formulation, although it is somewhat phenomenological and suffers from theoretical difficulties.¹⁰ However, to some extent, it can explain many experimental results as, for instance, the inelastic interaction with impurity vibrational modes.⁸ The Hamiltonian of the MIM system is assumed to be¹⁵

$$H = H_a + H_b + \sum_{\vec{k}, \vec{k}', \vec{q}} T_{\vec{k}, \vec{k}', \vec{q}} C_{\vec{k}}^{\dagger b} C_{\vec{k}'}^a + \text{h. c.},$$

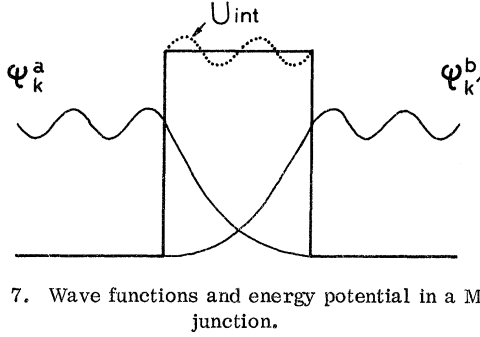


FIG. 7. Wave functions and energy potential in a MIM junction.

where $H_{a,b}$ are the Hamiltonians of the electrodes a, b without coupling, the last terms are the transfer Hamiltonian, and $C_{\vec{k}}^{a,b}$ are the electron-creation operators of wave vector \vec{k} in the corresponding electrodes. By considering the transfer Hamiltonian as a perturbation, we obtain the transition probability between initial and final states which describe the electrons and the barrier. The matrix element $T_{\vec{k}\vec{k}';\vec{q}}$ includes two terms:

$$T_{\vec{k}\vec{k}';\vec{q}} = T_{\vec{k}\vec{k}';\vec{q}}^0 + \delta T_{\vec{k}\vec{k}';\vec{q}},$$

where $T_{\vec{k}\vec{k}';\vec{q}}^0$ involves only electron states and $\delta T_{\vec{k}\vec{k}';\vec{q}}$ also involves barrier-phonon states with wave vector \vec{q} .

Then, to calculate explicitly the elastic and inelastic currents, we need the matrix element $T_{\vec{k}\vec{k}';\vec{q}}$. In a way which is analogous to the Bardeen approach,¹⁵ it is assumed that

$$T_{\vec{k}\vec{k}';\vec{q}} = \int_{\text{bar}} d^3r \langle f | \psi_{\vec{k}'}^a | H_0(r) + u_{\text{int}}(r) | \psi_{\vec{k}}^b \rangle | 0 \rangle,$$

where $|0\rangle$ and $|f\rangle$ are phonon states, $\psi_{\vec{k}}^a$ and $\psi_{\vec{k}'}^b$ are electron wave functions located in the a and b electrodes, with an exponential tail in the barrier, and $H_0 + u_{\text{int}}$ is the total Hamiltonian in the barrier, including the electron-phonon interaction (see Fig. 7). This gives us, for the elastic and inelastic matrix elements,

$$T_{\vec{k}\vec{k}';\vec{q}}^0 = \phi d e^{-Kd} \delta_{\vec{k}_{\parallel}, \vec{k}'_{\parallel}},$$

$$\delta T_{\vec{k}\vec{k}';\vec{q}} = D_{\vec{q}} \frac{e^{iq_x d} - 1}{iq_x} e^{-Kd} \delta_{\vec{k}_{\parallel}, \vec{k}'_{\parallel} + \vec{q}_{\parallel}},$$

where d and ϕ are the thickness and the height of the barrier; K is defined as $\hbar^2 K^2 / 2m^* = \phi - E_x$, where m^* is the electron mass and E_x the x component of its energy; $D_{\vec{q}}$ is the matrix element of the electron-phonon interaction in the insulator; q_x and \vec{q}_{\parallel} are the two components of the phonon wave vector. The Kronecker symbol gives the conservation of \vec{k}_{\parallel} for the electron-phonon system.

Then, the current densities are

$$I^{e1} = \frac{em^* \phi^2 K_0 d}{8\pi^2 \hbar^3 E_F} e^{-2K_0 d} eV,$$

$$I^{\text{inel}} = \sum_{\vec{q}} \frac{|D_{\vec{q}}|^2}{\phi^2} \frac{q_x^{-2}}{d^2} |e^{iq_x d} - 1|^2 \times I^{e1} (eV - \hbar\omega_{\vec{q}}) \theta(eV - \hbar\omega_{\vec{q}}),$$

where K_0 corresponds to $E_x = 0$, E_F is the Fermi energy of the metals that we assume to be identical, V is the applied voltage, and θ is the unit step function. Assuming a random orientation of the MgO crystallites, we take an average over the \vec{q} directions. The second derivative of the total current becomes

$$\frac{d^2 I}{d(eV)^2} = \frac{\sigma_0}{e} \sum_{\vec{q}} \frac{|D_{\vec{q}}|^2}{\phi^2} f(qd) \delta(eV - \hbar\omega_{\vec{q}}),$$

where σ_0 is the conductance of the junction for the elastic current. The summation over the phonon branches μ is included in the symbol $\sum_{\vec{q}}$. The function $f(qd)$ comes from the overlap integral of the electron and phonon wave functions in the barrier; it is

$$f(\xi) = \frac{2}{\xi} \int_0^{\xi/2} \frac{\sin^2 t}{t^2} dt. \quad (3)$$

As MgO is essentially an ionic solid, we can assume that the electron-phonon interaction is a Coulomb one. So the square of the matrix element¹⁶ $D_{\vec{q}}$ is

$$|D_{\vec{q}}|^2 = \left(\frac{\hbar}{2N\omega_{\vec{q}}} \right) \left(\frac{2e^2}{v\epsilon_{\infty}} \right)^2 \times \sum_{\vec{G}} \left[\left(\frac{\vec{\epsilon}_{\vec{q}\mu}^+}{M_+^{1/2}} - \frac{\vec{\epsilon}_{\vec{q}\mu}^- e^{i\vec{G}\cdot\vec{b}}}{M_-^{1/2}} \right) \frac{\vec{q} + \vec{G}}{|\vec{q} + \vec{G}|} \right]^2 \frac{1}{(\vec{q} + \vec{G})^2 + q_0^2},$$

where v is the cell volume, ϵ_{∞} is the nonionic part of the dielectric constant, \vec{G} is a vector of the reciprocal lattice, $\vec{\epsilon}_{\vec{q}\mu}^{\pm}$ are the phonon eigenvectors relative to the ions Mg^{++} and O^{--} of the mass M_{\pm} . The vector \vec{b} gives the relative position of the two ions in the cell and q_0 gives the long-distance cutoff of the potential because of the image dipoles in the electrodes, $q_0 \sim \pi/d$. It should be noticed that for small \vec{q} the normal processes ($\vec{G} = 0$) are the most important, and then only the LO mode contributes. For large \vec{q} the contribution of the smallest \vec{G} vector is quite important and breaks this selection rule. The exact calculation of the umklapp contribution has not been done, but we have made an evaluation of it, assuming an isotropic distribution for the vectors $\vec{q} + \vec{G}$. The result for the second derivative of the current is

$$\frac{d^2 I}{d(eV)^2} = A \sum_{\vec{q}} \frac{1}{\omega_{\vec{q}}} \left\{ \left[\left(\frac{\vec{\epsilon}_{\vec{q}\mu}^+}{M_+^{1/2}} - \frac{\vec{\epsilon}_{\vec{q}\mu}^-}{M_-^{1/2}} \right) \frac{\vec{q}}{q} \right]^2 \times \frac{1}{q^2 + q_0^2} + \frac{5.6 \times 10^{-2} a^2}{M_+ + M_-} \right\} \times f(qd) \delta(eV - \hbar\omega_{\vec{q}}), \quad (4)$$

where

$$A = \frac{2e^3 \hbar \sigma_0}{Nv^2 \phi^2 \epsilon_0^2}$$

and a is the lattice parameter.

C. Comparison with Experiment

Using the eigendata from the work reported in Ref. 14, the spectrum can be calculated from Eqs. (3) and (4); the result is shown in Fig. 6(d). At low energy it is essentially the phonon density of states, but at *high energy*, the calculations lead to a *strong enhancement of the structure*. This result is in rather good agreement with the experiment: The central part of the spectrum (45–75 meV) fits the theoretical curve, and the peaks at 38 and 82 meV can be reproduced, to some extent, if we assume a broadening of the theoretical structure in that region.

It would be interesting to make these calculations within the framework of the new theory of Ref. 10; this is being attempted at the present time. But it already appears that there is a better fit of the experimental spectrum to the calculated curve than to the IR-absorption curve or to the phonon-density-of states plot [Figs. 6(b) and 6(c)]. It is pointed out that, as the selection rules [Eq. (4)] are different from those in IR, the inelastic-tunneling and IR-absorption spectra may be quite different. By tunneling in MgO, all the phonons are observed with an increased weight for the LO mode, whereas it is the TO mode alone that gives the IR absorption.

It may be instructive to compare our results to those of a recent experiment by Ladan and Zylbersztejn,¹⁷ in which they observe the phonon spectrum of amorphous germanium in Al-Ge-Sn junctions. Their experimental spectrum can be fitted, with good agreement, to the expression proposed by Bennett, Duke, and Silverstein¹⁸ for incoherent inelastic tunneling (induced by potential fluctuation):

$$\frac{d^2 I}{d(eV)^2} = B \frac{F(eV)}{eV},$$

where B is a constant and $F(E)$ is the phonon density of states. Such a law is clearly not valid in the case of MgO, as it would completely miss the high-energy part of our spectrum (LO modes). This emphasizes the difference between the coupling of tunneling electrons with phonons in a crystalline and ionic barrier, and the corresponding coupling in an amorphous and covalent one.

The identification of the spectrum from the phonon data of MgO leaves little ambiguity about the chemical composition of the insulator. The tunnel barrier grown on Mg appears to be MgO. This is in contrast to the insulator grown on Al that was concluded to be Al(OH)₃ by Geiger *et al.*¹⁹ A

confirmation of this difference is found by studying the spectrum about 120 meV. If water vapor is introduced during the oxidation process, in both types of junctions there is a peak in that region which is attributed to an OH bending mode. But, if an oxidation is done, without introducing water, this peak is eliminated in Mg junctions, whereas, with junctions on Al, such an operation has not yet succeeded in eliminating the bending mode. This seems to indicate that the hydroxide is necessary to make the barrier on Al.

D. Oxygen Isotopic Effect

The isotopic effect is a powerful tool used in spectroscopy to identify a structure. Regarding the minute quantity of material used to make a tunnel barrier, we see, for example, that it is possible to perform an experiment with O¹⁸ instead of O¹⁶ (whereas it would be impossible in a neutron-scattering experiment, as large crystals are necessary). We have made the junctions in the usual way, but introduced O¹⁸ during the oxidizing discharge.²⁰ The resulting MgO phonon region of the spectrum is shown in Fig. 8. Besides the structure we have already met with O¹⁶, a new series of peaks appears which is slightly shifted with respect to the 66- and 82-meV lines (respectively, 62.8 and 78.8 meV). The existence of a double series of peaks indicates that we have not succeeded in eliminating the O¹⁶ isotope, probably because of some isotopic exchange of the O¹⁸ gas in the bell jar.

Experimentally, the isotopic shifts $[(\omega_{16} - \omega_{18})/\omega_{16}]$ that we find for these two lines are, respectively, 4.9 and 3.9%. Now, the calculations of Sec. IV B can be performed with a mass of 18 for the oxygen, and the isotopic effect predicted. In the 0–60-meV region the spectrum found does not differ appreciably from that found with O¹⁶, but the 66- and 82-meV lines are shifted, respectively, by 5.6 and 3.4%.²¹ The agreement between the measured values and the calculated ones appears to be rather good, however the validity of such a comparison is questionable as, in the O¹⁸ experiment, two types of oxygen atoms are present, and some coupling between the corresponding oscillators may exist. Nevertheless, this isotopic effect gives a new support to the hypothesis that the magnesium oxide is responsible for the structure in the 30–100-meV range of the spectrum.

V. VIBRATIONAL MODES OF MOLECULAR IMPURITIES IN DOPED JUNCTIONS ($eV > 100$ meV)

As they indicate in their paper,² Lambe and Jaklevic have not tried to make a detailed analysis of their spectrum—they have just given a general interpretation of the curves according to the radicals which were introduced. It is interesting to

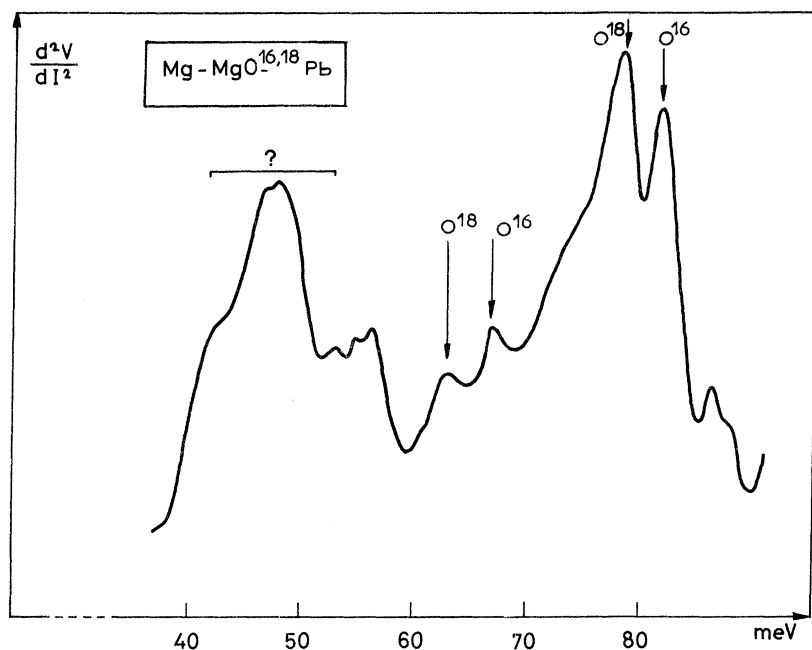


FIG. 8. Isotopic effect: spectrum of a MgO barrier made by oxidation in O^{18} .

know whether the agreement with the IR data is accurate enough to allow a real identification of the molecules or not. We shall present a few studies in which this identification seems to be possible.

A. Al-Pb Junction Doped with Formic Acid

When an acid gas is introduced during the oxidation process of a junction, the resulting structure in the spectrum is very strong. This indicates that the molecules of the acid are absorbed in the oxide at a high rate—probably because they make a chemical bond with the oxide. We can try to test this idea by studying the spectrum in detail. On the other hand, the carboxylic acids, and especially formic acid, easily give dimer molecules, thanks to H bonds. So it is also interesting to know what is the state of the molecules within the barrier: Do they correspond to a monomeric or dimeric acid, or to an aluminum salt?

The spectrum found by the exposure of a freshly oxidized Al film to the vapor of formic acid is represented in Fig. 9. Assuming that the acid introduced in the bell jar deposits uniformly on the surfaces, we estimate the number of molecules in the junction ($0.1 \times 0.1 \text{ mm}^2$) to be 3×10^{10} . This corresponds to a very high sensitivity for spectroscopy.

Table I gives the comparison between the spectrum and IR data for the monomeric²² and dimeric²³ acids and for the sodium salt.²³ Let us examine successively how to interpret the different observed peaks.

447 meV. This corresponds to the stretching mode of OH. The energy is roughly the same as

in the monomer, but this is not conclusive, as this peak is already present for nondoped junctions. However, we can already conclude the *absence of dimer molecules*, as these molecules would give a typical band in the 372–310-meV region²⁴ and the spectrum clearly lacks such a structure.

370.5–353–338 meV. This triplet is associated with the stretching of CH. In that region, monomeric or dimeric acid presents a broad peak cen-

TABLE I. Identification of the spectrum shown in Fig. 9. The features of the peaks are weak (w), middle (m), strong [(s), and figure underlined)], and broad (b). The IR data for sodium salt, dimeric acid, and monomeric acid are taken from Refs. 23 and 22.

Tunneling spectrum (meV)	Infrared data (meV)			Identification
	sodium salt	dimeric acid	monomeric acid	
447		broad band 372–310	442	ν O-H matrix ?
{ 370.5 (w) 353 (s) 338 (w)	{ 365 350 336	{ 367	{ 365	ν C-H
	221	
199 (m)	210	α
182 (w)	200	
171 (s)	170.5	173	173	COO ⁻
144	...	149	149	s
	136.4	
130 (s)	131	130		ν C-O
116 (s, b)				matrix (δ O-H)
81		83	81.5	δ OCO

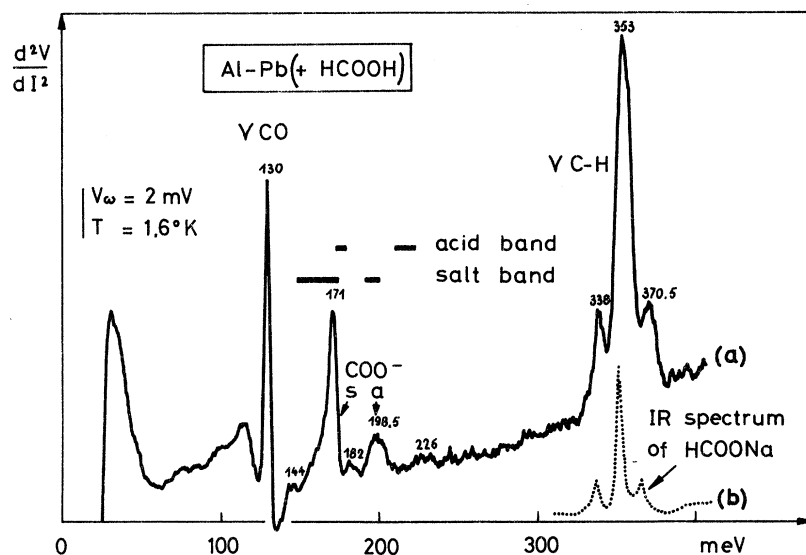


FIG. 9. (a) Tunneling spectrum of an Al-Pb junction doped with formic acid. The locations of the vibrational bands of the carboxylic groups, deduced from IR spectroscopy, are reported above the experimental curve. The values for salts and acids are well separated and permit an identification of the molecules included in the barrier as being salt molecules. The energies of the different peaks are marked on the curve, and the identification of the corresponding modes is discussed in Table I. (b) Stretching modes of the C-H group obtained by IR spectroscopy on sodium formiate.

tered about 365 meV. This identification is not convincing because of the energy of the center of the structure and its resolution into a triplet. In contrast, the agreement with the spectrum of the sodium formiate is quite remarkable [see curve (b)]. So it is concluded that the main compound is a *salt of formic acid with aluminium*.

199–171 meV. This is the other important region for the identification of carboxylic acids. The COOH group gives absorption at 221 and 173 meV for the monomer and 210 and 173 meV for the dimer, and, as a rule, the high-frequency mode is always above 210 meV for saturated acids. However, when the group is ionized, as in salts, the antisymmetrical and symmetrical modes of $O=C=O^-$ are located at energies from 200 to 192 meV and 174 to 149 meV.²⁴ This gives us a valuable tool for identification. As can be seen in Fig. 8, we have a *confirmation of the presence of the ionized radical*.

130–116–81 meV. The sharp peak at 130 meV corresponds to a region where a structure is always met with carboxylic groups. It is generally attributed to a CO stretching. However, we are not very satisfied with this identification. The 116-meV mode is already present in the matrix and is an OH bending vibration of the aluminium hydroxide, which is probably the main compound of the "oxide" barrier.¹⁹ The absence of the 81-meV peak in the salt spectrum and its presence in that of the acids are not significant, as the data we have for the salt are less resolved than for acids in that region.

In conclusion, the study of the spectrum formed with formic acid gives us a clear indication of the state of molecules inside the barrier. Most of them are chemically bound to the aluminium hy-

droxide, and this explains the strong rate of absorption of the acid in the junctions. Notice that this information is obtained from two independent determinations (C-H stretching and COO^- stretching).

A similar study of the acetic acid CH_3COOH leads to similar conclusions, with, in addition, the identification of the $-CH_3$ radical with elimination of carbon with nonsaturated bond and of $-CH_2^+$ radicals.

B. Water-Doped Mg-Pb Junction: Isotopic Effect. Specific Features

The recorder plot of a Mg-Pb junction, doped with water and heavy water, is shown in Fig. 10. Both stretching modes of OH and OD are observed, with a strong maximum, respectively, at 333 and 451 meV. The two line shapes are similar; the OH peak, for instance, is included in the interval 433–461 meV.

The isotopic shift is of the order of $2^{1/2}$, as has already been observed by Lambe and Jaklevic² in Al-Pb junctions. But, as the lines are sharp in that type of junction, we can try to make an accurate measurement of the isotopic shift, as is extensively done in molecular physics to identify species. The experimental ratio we find is: $\omega_{OH}/\omega_{OD} = 1.355 \pm 0.004$. This value is rather different from $2^{1/2} = 1.414$, which would correspond to a harmonic oscillator with the oxygen atom motionless during the vibration. It is also slightly different from the reduced-mass ratio: $(\mu_{OD}/\mu_{OH})^{1/2} = 1.374$. But it fits the values for free OH molecules (1.356) or for OH^- impurities in a rare-gas matrix (1.357).^{25,26} However, it also agrees with the value for the internal vibration of OH radicals in a lattice of $Mg(OH)_2$ (1.360).²⁷ So, in

that specific case, the OH-OD isotopic effect has been obtained with rather good precision, but it is still not accurate enough to enable us to identify the molecular species.

Nevertheless, such an identification can be attempted, thanks to the absolute position of the lines. The comparison with OH⁻ impurities in a MgO crystal can be done thanks to the infrared study by Glass and Searle.²⁸ They observe a line at 410 meV and a second one between 440 and 460 meV according to the crystallographic situation of the impurities. The lack of the first line is enough to eliminate this identification. The spectrum is then compared to the infrared absorption of the brucite, Mg(OH)₂. From Refs. 27 and 29, the two internal stretching modes of the OH radicals are located at 453 and 459 meV. There is an agreement with our data, as those two energies are included in the linewidth of our peak. So it seems likely that the presence of water during the oxidation process has led to the formation of hydroxide molecules in the 30-Å-thick barrier. But further investigations may be useful to confirm this result.

Anyway, the spectrum already gives us a definite

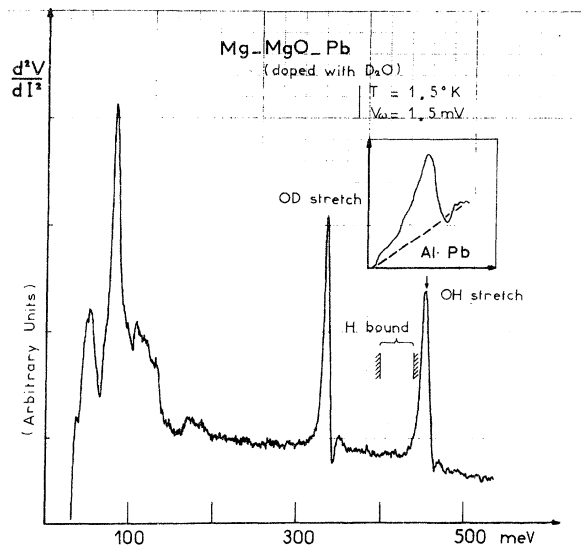


FIG. 10. Recorder plot of the second derivative of the tunneling current for a Mg-MgO-Pb junction doped with H₂O and D₂O. The arrow, above the curve, corresponds to the energy of the stretching vibrational mode of a free OH radical (no hydrogen bond). At lower energy the bracket corresponds to the energy band of this mode, when there are hydrogen bonds of the radical with the surrounding. It is deduced that the OH group in MgO has no hydrogen bond. In order to make a comparison, the line of the OH stretching, in an Al-Pb junction, is shown in the inset; the situation appears to be quite different, as the peak has a long tail in the H bond region. Notice the undershoot after the OD and OH stretching peaks in the Mg-Pb junction.

information: *The hydrogen atoms are just bound to a single oxygen.* If there were hydrogen bonds with the surrounding, the stretching mode would be typically shifted to lower energies,²⁴ as is indicated in Fig. 10. It is pointed out that the situation of the OH stretching is different in Al-Pb junctions, as can be seen in the upper part of Fig. 10. In that case, the OH peak has a large low-energy tail, indicating the presence of H bonds.

C. Effect of Superconducting Electrode on Vibrational Mode Line Shape

In the conditions of our experiment, if we examine carefully the line shape of a sharp and well-defined mode, as the OD stretching, we can observe an undershoot on the high $|V|$ side of the peak (Fig. 10). In a tunneling experiment, the physical origin of any structure associated with vibrations of the system is somewhat ambiguous: It may be either a self-energy effect or an inelastic effect. The usual criteria to distinguish between the two are the parity of the structure and its general shape. Inelastic effects give "pure" peaks, and renormalization leads to peaks with a large undershoot in the second derivative of the current. In practice, the distinction between the two is not often so clear, because of the background of the tunneling characteristics. In our case, we could have thought of a mixed origin of the structure. However, Duke and Kleiman³⁰ have done a recent calculation for a metal-semiconductor junction (but also valid in the case of MIM structure) which gives a criterion for deciding between the two possible origins of the structure. To apply this criterion, one considers the modification of the structure when one electrode is driven in the normal state by applying a magnetic field. If the structure is connected with renormalization effect, there is no notable modification of the experimental curve. But, if it is due to inelastic effect, the undershoot must vanish. This is what is actually observed in our experiment [Figs. 11(a) and 11(b)]. This confirms what is generally admitted—that the molecular impurities structure is due to inelastic tunneling.

Now we can calculate the expected effect of superconducting electrodes on the line shape of an excitation, within the framework of the inelastic-tunneling theory. The inelastic part of the current, at $T = 0^\circ\text{K}$, can be written⁸

$$I_{inel} = K \int_{-\infty}^0 d\omega_1 \int_0^{+\infty} d\omega_2 N_T(\omega_1) D(\omega_1 - \omega_2 + eV),$$

where K is a constant, ω_1 and ω_2 are the electronic energies, respectively, in the lead and magnesium electrodes, $D(\omega_1 - \omega_2 + eV)$ is the dipole spectral weight function of the OD group (this function is peaked at the energy of the stretching mode); and $N_T(\omega_1)$ is the effective tunneling density of

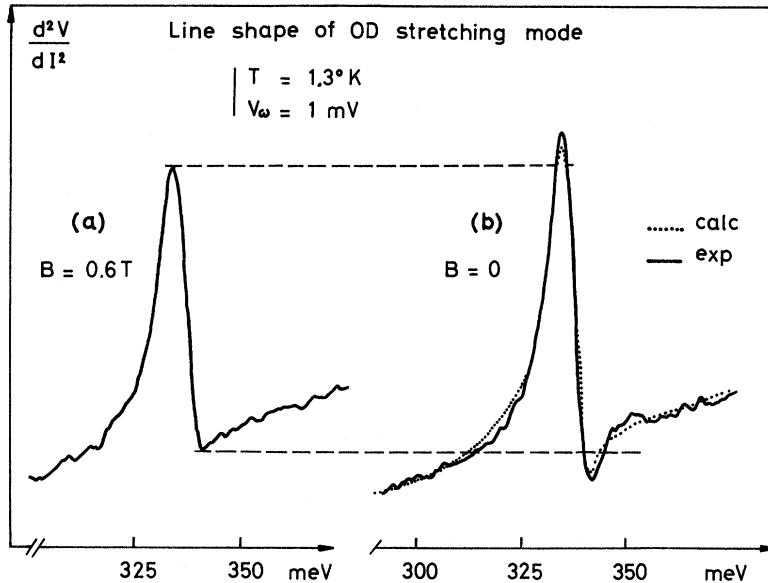


FIG. 11. Detail of the line shape of the OD stretching mode in a Mg-Pb junction. (a) Pb is normal, (b) Pb is superconducting. The dotted curve is the line shape calculated for a superconducting Pb electrode, by using the spectral weight function of the OD mode from curve (a) and a BCS density of states for the superconducting Pb.

states of the superconducting (or normal) Pb. The experimental data involve the second derivative of the tunneling current which is

$$\frac{d^2 I_{\text{inel}}}{d(eV)^2} = K \int_0^\infty \dot{D}(\omega_0) \frac{dN_T}{d\omega} (eV - \omega_0) d\omega, \quad (5)$$

where $dN_T/d\omega$ is a δ function when Pb is normal, and can be approximated with the BCS expression when it is superconducting. Then, as the normal characteristic [Fig. 11(a)] gives us the dipole weight function $D(\omega_0)$, we can calculate the line-shape change when the Pb electrode is driven from the normal state to the superconducting state by applying a magnetic field. In Fig. 11(b) we have reported the experimental line of the OD stretching mode with a superconducting Pb electrode, and the result of the calculation performed from Eq. (5). The agreement between the two is fairly good and we think that most of this structure is correctly explained by this approach. In fact, such a modification of the line shape was expected, according to Lambe and Jaklevic,² but it is the first time that it has been quantitatively observed.

V. CONCLUSION

Inelastic electron tunneling appears to be a type of spectroscopy that can give interesting information about the vibrations of all the component parts of the MIM system.

The phonons of the electrodes are observed. At the present time there is no explicit theory

which can predict the experimental spectrum. However, it seems that most of the structure can be explained as representing the phonon density of states of the electrodes. And it seems, at least in some cases, that this determination of the density is competitive with respect to other determinations. We have shown that the tunneling current is a *short-range probe of this phonon density* in the electrodes.

The phonons of the barrier lattice also give a definite structure in the $d^2 I/dV^2$ characteristic. The study of junctions with MgO has shown that the weight which must be assigned to the different phonons of the barrier to get the tunneling spectrum is quite different from that which must be used to get the IR-absorption spectrum of the same material. Thus, it is pointed out that any direct comparison between the two types of spectra may be misleading.

About the spectroscopy of the molecular impurities contained in the barrier, it appears that it is more accurate, in identifying the molecules, than might at first have been thought. Careful studies of the energy and of the line shape of the peaks can give interesting information on the nature of the impurities and on their chemical binding with the insulating matrix. The example of junctions doped with formic acid demonstrates these possibilities. In the future, such studies may provide useful tool in the problem of adsorption on solid surfaces, because it is a spectroscopic method which is sensitive to thicknesses of very few atomic layers.

*Work supported in part by the Direction des Recherches et Moyens d'Essais, Contract No. 70/147.

¹R. C. Jaklevic and J. Lambe, Phys. Rev. Letters **17**, 1139 (1966).

- ²J. Lambe and R. C. Jaklevic, *Phys. Rev.* **165**, 821 (1968).
- ³R. C. Jaklevic and J. Lambe, *Bull. Am. Phys. Soc.* **14**, 43 (1969); J. Klein and A. Léger, *Phys. Letters* **28A**, 134 (1968); J. M. Rowell, W. L. McMillan, and W. L. Feldmann, *Phys. Rev.* **180**, 658 (1969); P. Guélin and G. Schröder, *Solid State Commun.* **8**, 291 (1970).
- ⁴J. G. Adler, *Phys. Letters* **29A**, 675 (1969).
- ⁵I. Giaever and H. R. Zeller, *Phys. Rev. Letters* **21**, 1385 (1968).
- ⁶J. G. Adler, *Solid State Commun.* **7**, 1635 (1969).
- ⁷R. C. Jaklevic and J. Lambe, *Phys. Rev. B* **2**, 808 (1970).
- ⁸D. J. Scalapino and S. M. Marcus, *Phys. Rev. Letters* **18**, 459 (1967).
- ⁹There may appear to be some ambiguity in the 16-meV peak because the Au longitudinal-phonon energy is also in this range. However, a study of Al-Au junctions indicates that the Au phonon structure is much weaker than what is observed here.
- ¹⁰C. Caroli, R. Combescot, P. Nozières, and D. Saint-James, *J. Phys. C* **5**, 21 (1972).
- ¹¹J. Young and J. Koppel, *Phys. Rev.* **134**, A1476 (1964).
- ¹²A. Léger and J. Klein, *Phys. Letters* **28A**, 751 (1969).
- ¹³It should be noticed that the electronic mean free path is always larger than the thickness of metal (1). In the case of Pb, for electrons whose energy is $E \sim \Theta_{\text{pb}}$, McMillan and Rowell evaluate the value to be 500 Å [*Superconductivity*, edited by R. D. Parks (Marcel Dekker, New York, 1969), p. 581]. This points out the difference between the electronic mean free path and the range of the inelastic-tunneling probe.
- ¹⁴M. J. L. Sangster, G. Pekham, and D. H. Saunderson, *J. Phys. C* **3**, 1026 (1970).
- ¹⁵C. B. Duke, *Tunneling in Solids* (Academic, New York, 1969), p. 207.
- ¹⁶See, for instance, J. R. Schrieffer, *Theory of Superconductivity* (Benjamin, New York, 1964), Chap. IV; C. G. Kuper and G. D. Whitfield, *Polarons and Excitons* (Oliver and Boyd, Edinburgh, 1962).
- ¹⁷F. Ladan and A. Zylbersztejn, *Phys. Rev. Letters* **28**, 1198 (1972).
- ¹⁸A. J. Bennett, C. B. Duke, and S. D. Silverstein, *Phys. Rev.* **176**, 969 (1968).
- ¹⁹A. L. Geiger, B. S. Chandrasekhar, and J. G. Adler, *Phys. Rev.* **188**, 1130 (1969).
- ²⁰The O¹⁸ isotope was supplied by the Weizmann Institute (Rehovot).
- ²¹This value corresponds to the square root of the reduced-mass ratio as it is expected for optical phonons of zone center.
- ²²G. Herzberg, *Infra-red and Raman Spectra of Polyatomic Molecules* (Van Nostrand, New York, 1945), p. 321.
- ²³J. Gupta, *Indian J. Phys.* **10**, 118 (1936).
- ²⁴L. J. Bellamy, in *The Infra-red Spectra of Complex Molecules* (Methuen, London, 1966).
- ²⁵G. Herzberg, *Spectra of Diatomic Molecules* (Van Nostrand, New York, 1950), p. 560; N. Acquista, L. Schoen, and D. Lide, *J. Chem. Phys.* **48**, 1534 (1968).
- ²⁶There is a difference between the isotopic effect for OH-OD free molecules and the square root of the reduced-mass ratio, because the vibrators are anharmonic.
- ²⁷R. A. Buchanan, H. H. Caspers, and J. Murphy, *Appl. Optics* **2**, 1147 (1963).
- ²⁸A. M. Glass and T. M. Searle, *J. Chem. Phys.* **46**, 2092 (1967).
- ²⁹S. S. Mitra, in *Solid State Physics*, edited by F. Seitz and D. Turnbull (Academic, New York, 1962), Vol. 13, p. 1.
- ³⁰C. B. Duke and G. G. Kleiman, *Phys. Rev. B* **2**, 1270 (1970).

Optical Absorption in the Alkali Metals: Detailed Calculations

D. J. Stevenson*

Victoria University of Wellington, New Zealand

(Received 10 August 1972)

The results of detailed computations of the optical absorption in alkali metals are presented. Nettel's formalism is used to calculate the phonon-assisted processes and modifications are made to allow approximately for the Debye-Waller factor, multiphonon terms, anharmonic effects, and the "optical pseudopotential." The direct interband absorption is also incorporated, and the validity of the classical ω^{-2} frequency dependence for the Drude absorption is discussed. Results are presented as a function of temperature, form factor, and pseudopotential coefficient V_{110} . Smith's data for absorption in sodium are found to be consistent with $V_{110}(0^\circ\text{K}) = 0.28$ eV. The data for potassium and rubidium are also consistent with the model but the data for cesium and lithium are not.

I. INTRODUCTION

In recent years, there have been many experimental and theoretical investigations of the optical properties of the alkali metals. Despite this intensive activity, quantitative disagreement between

experiment and theory remains. The objective of the present work is to examine whether the discrepancies can be explained without abandoning the single-particle formalism. In particular, the effect of phonons on the absorption is considered quantitatively. Recent papers¹⁻³ have emphasized